AFGL-TR-82-0103

MULTICHANNEL VUV ROCKETBORNE MONOCHROMATOR
FOR LOW-LEVEL AURORAL MEASUREMENTS

Henry A. Miranda, Jr.

EPSILON LABORATORIES, INC.
4 PRESTON COURT
BEDFORD, MASSACHUSETTS 01730

MARCH 1982

Final Report for Period 14 February 1979 through 01 March 1981

AIR FORCE GEOPHYSICS LABORATORY
AIR FORCE SYSTEMS COMMAND
UNITED STATES AIR FORCE
HANSCOM AFB, MASSACHUSETTS 01731

DTIC
ELECTE
JUN 21 1982
S   D
B

82 06 21 09

REPORT DOCUMENTATION PAGE		READ INSTRUCTIONS BEFORE COMPLETING FORM
1. REPORT NUMBER AFGL-TR-82-0103	2. GOVT ACCESSION NO. ADA115 815	3. RECIPIENT'S CATALOG NUMBER
4. TITLE *(and Subtitle)* MULTICHANNEL VUV ROCKETBORNE MONOCHROMATOR FOR LOW-LEVEL AURORAL MEASUREMENTS		5. TYPE OF REPORT & PERIOD COVERED Final 14FEB79 – 01MAR81
		6. PERFORMING ORG. REPORT NUMBER
7. AUTHOR(s) Henry A. Miranda, Jr.		8. CONTRACT OR GRANT NUMBER(s) F19628-79-C-0019
9. PERFORMING ORGANIZATION NAME AND ADDRESS Epsilon Laboratories, Inc. 4 Preston Court Bedford, MA 01730		10. PROGRAM ELEMENT, PROJECT, TASK AREA & WORK UNIT NUMBERS 62101F 660916AC
11. CONTROLLING OFFICE NAME AND ADDRESS Air Force Geophysics Laboratory Hanscom Air Force Base, MA 01731 Monitor: R. Van Tassel/LKO		12. REPORT DATE March 1982
		13. NUMBER OF PAGES 22
14. MONITORING AGENCY NAME & ADDRESS *(if different from Controlling Office)*		15. SECURITY CLASS. *(of this report)* Unclassified
		15a. DECLASSIFICATION/DOWNGRADING SCHEDULE

16. DISTRIBUTION STATEMENT *(of this Report)*

Approved for public release; distribution unlimited.

17. DISTRIBUTION STATEMENT *(of the abstract entered in Block 20, if different from Report)*

18. SUPPLEMENTARY NOTES

(Cupt)

19. KEY WORDS *(Continue on reverse side if necessary and identify by block number)*

Monochromator
Multichannel monochromator
VUV
Rocketborne VUV detector

Photon counting
Auroral detector

20. ABSTRACT *(Continue on reverse side if necessary and identify by block number)*

A multichannel photon counting VUV monochromator is described whose
design features high sensitivity, rugged construction within about
a 2/3 ft³ volume, and low crosstalk. Discussed also are the details
of a careful calibration, as well as the results of a very preliminary
analysis of data collected on a rocket flight into an aurora in March
of 1981.

(See reverse side)

DD FORM 1473 1 JAN 73   EDITION OF 1 NOV 65 IS OBSOLETE

i

20. Abstract cont'd.

It is concluded that the basic design of the instrument is valid. In addition, arguments are advanced to support the view that, in spite of the unfortunate use of a high-scattering grating, valid auroral emission rate data may have been collected in the 1325 Å, 1356 Å and 1384 Å channels.

SUMMARY

A multi-channel photon counting VUV monochromator featuring high
sensitivity with 10 Å (FWHM) passband, and rugged design within a modest
volume (slightly larger than 2/3 cubic ft.), kinematic mounting, and low
crosstalk between channels has been developed under this contract. This
instrument incorporated five channels, 1200 Å, 1216 Å, 1325 Å, 1356 Å, and
1384 Å, the spacing between which in the focal plane was such as to require
special light guide assemblies beyond the exit slits. These are of two
varieties: the straight-through and the right-angle folded. The straight-
through variety increases the overall system sensitivity, whereas the
folded variety, because of the extra reflection, suffers a net loss in
sensitivity.

Unfortunately, the grating procured for this specific device exhibited
unusually high scattering properties which masked a good deal of the signals,
owing to the relatively high-level 1304 Å atomic oxygen signal characterist-
ically present in all auroral events. Since this deficiency was not dis-
covered early enough to permit the procurement and installation of a suit-
able substitute grating, a calcium fluoride window was installed in front of
the entrance slit. Thus the 1200 Å channel was sacrificed by converting it
to the measurement of scattered light in the remaining channels.

The instrument was flown in early March of 1981 to an apogee of 158 km
as part of a Taurus-Orion payload during a diffuse aurora, and VUV data
were collected. A preliminary analysis of the signals was conducted in
order to assess the operation of the system under flight conditions. On the
basis of this analysis, together with the results of a careful series of
tests performed at both the AFGL and Johns Hopkins VUV calibration facil-
ities, it is concluded that the system functioned as anticipated. Moreover,
in spite of excessive scattering it is believed that useful auroral emission
rate information may have been obtained with regard to the (4,0) and (2,0)
LBH transitions at 1325 Å and 1384 Å, respectively.

TABLE OF CONTENTS

1.0 INTRODUCTION

This report describes a rocketborne multi-channel VUV monochromator developed under this contract. A five-channel configuration was used for this particular experiment, however, the system can readily accommodate additional channels to suit the specific requirements and/or priorities of a given experiment, within certain easily identifiable bounds.

The instrument was designed to use the available space within the volume and weight constraints of a Taurus-Orion payload. The process of converging toward the final system involved several design iterations during the course of the program. A significant element was the requirement for a special photomultiplier encapsulation package of very small volume. This particular development effort resulted in a photon-counting PM detector module housed within a parallelepiped as small as 22mm x 50mm x 110mm. Each such module incorporated an EMR 510 PM tube, together with all of the ancillary HV power supply components as well as the preamplifier and pulse shaping circuitry and connectors, etc., and produced output pulses compatible with standard on-board telemetry hardware. It is of interest to note that the PM tube itself occupied more than half of the total volume of each module.

The basic instrument design incorporates several inherent features that are desireable for auroral experimentation in the UV and VUV regions of the spectrum where the data are often characterized by weak signals from relatively narrow fields of view. Among these features are: high sensitivity and rugged construction within a modest volume ($26\frac{1}{2}$" x 8.3" x 6.0"), kinematic mounting to provide isolation from payload flexations, and low cross talk between adjacent channels. Unfortunately, this latter feature was not realized because the particular Bausch and Lomb grating procured for the instrument exhibited an unusually high scattering component, 10-50 times that which is normally anticipated. Due to several program delays the discovery of this particular deficiency did not take place early enough to permit the procurement of a suitable alternative grating in time to meet the rocket launch schedule.

In spite of these difficulties however, it is believed that meaningful auroral VUV data may have been obtained during the rocket flight. Moreover, the validity of the basic design features, having been substantiated by a careful series of laboratory tests, warrant description here because with relatively trivial modifications it could serve as an adjunct to extant instrumentation.

The Ground Support Equipment (GSE) recorded the outputs of all channels on a commercial tape cassette, and permitted the sequential readout of the recorded integral photon counts in any of the five channels, as well as the PM tube high voltage and selectable integration time. This device was tested and used to good advantage both during the calibration effort and for checkout prior to launch.

2.0 DESCRIPTION OF INSTRUMENT

2.1 Configuration

The device as shown in Figure 1 is a modified, Ebert-Fastie design employing a single large mirror, an entrance slit centrally located above the plane grating with exit slits below. The line joining the centers of these slits is symmetrically located with respect to the center of the entrance slit about the horizontal mid-plane of the system. The mirror is cut in a trapezoidal shape so as to minimize the volume occupied by the system.

The system is attached to the rocket payload mounting platform at three points: two bolts in the rear, and a pin within a front mounting hole to permit differential thermal expansion between the system and the payload without introducing undue torques upon the instrument. The design employed five output channels: 1200 $\overset{o}{A}$, 1216 $\overset{o}{A}$, 1325 $\overset{o}{A}$, 1356 $\overset{o}{A}$ and 1384 $\overset{o}{A}$. Each channel was provided with a separate PM detector module so as to yield five simultaneous continuous outputs, thereby avoiding the complexities and S/N degradation associated with multiplexed or sequentially-scanned outputs. All of the modules are mounted onto a shelf cantelivered from the front wall. The grating is mounted on the back of this wall.

As can be seen from the figure, two of the five channels are sandwiched in between the other three, and oriented vertically instead of horizontally. This was done because the lateral separation of the wavelengths for the experiment was smaller than the least dimension of the modules.

2.2 Light Guides

Each detector module is connected optically to its respective monochromator exit slit through a light guide. This performs two tasks: 1) it couples the rectangular slit dimension to the circular 6mm diameter PM tube photocathode surface, and 2) offsets the latter by a sufficient distance to permit the vertically-oriented alternating module light guides, which fold the exit beam through 90°, to be fitted in. Schematic layouts of both types are shown in Figure 2. These indicate that most of the axial pencils diverging from the focal plane are collected onto the photocathode after only one reflection for the straight-through channels. In the case of the folded-light channels, two reflections are required, and also a slightly larger proportion of diverging pencils will require three reflections.

A great deal of effort was expended in designing and fabricating these light guides. Originally, it was intended to use glass surfaces with appropriate aluminization and overcoating for VUV application. Unfortunately, a suitable bonding agent could not be found that would meet the simultaneous demands imposed by the anticipated thermal stresses (to about -50°C) as well as the necessity of avoiding outgassing under vacuum conditions and attendant deposition of unwanted absorption in the optical surfaces.

TOP VIEW

Entrance Slit Assembly

Grating Assembly

Baffles

Mirror

PMT Modules

Front View

Light Guides

Front Mounting point

SIDE VIEW

Mounting platform

Rear Mounting Points
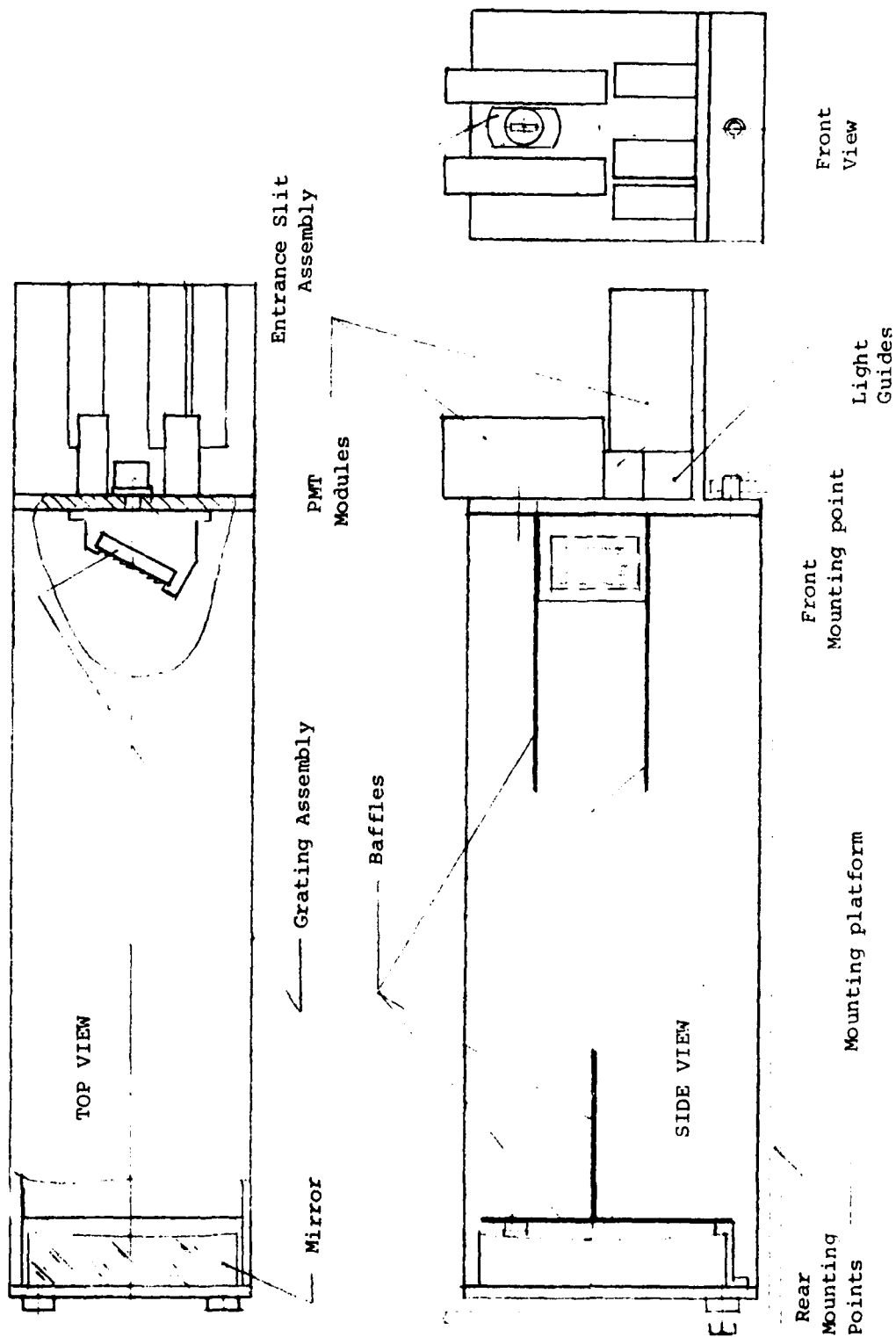
FIGURE 1: VUV Monochromator Schematic Layout

AXIAL
VIEW

STRAIGHT-THROUGH
LIGHT GUIDE STRUCTURE

PM TUBE
CATHODE

SIDE
WALLS

FOCAL PLANE
(EXIT SLIT)

BEAM-FOLDING
LIGHT GUIDE
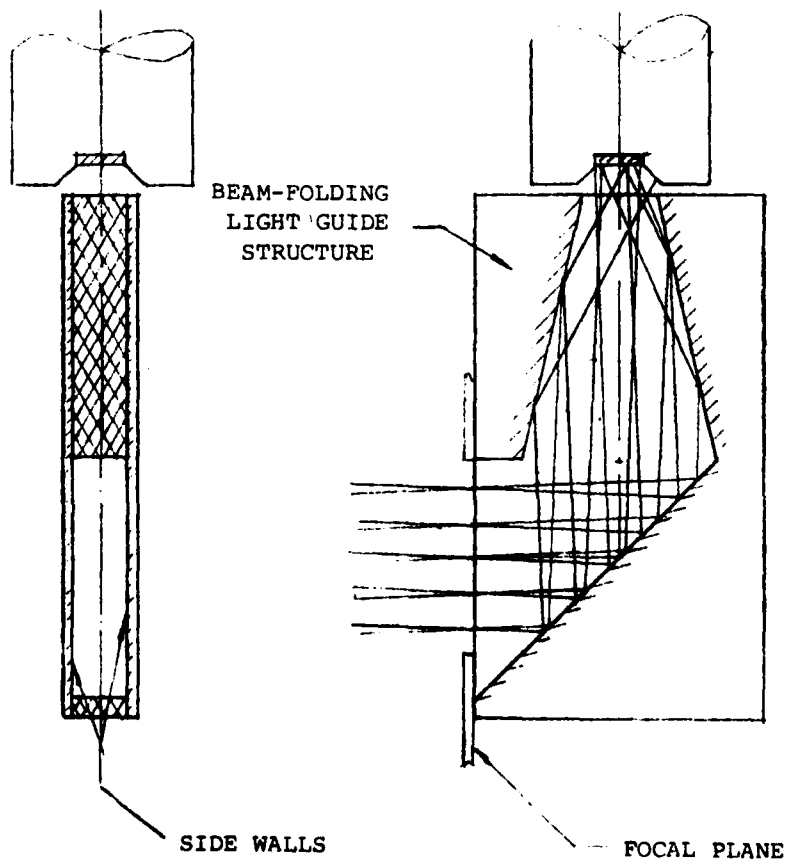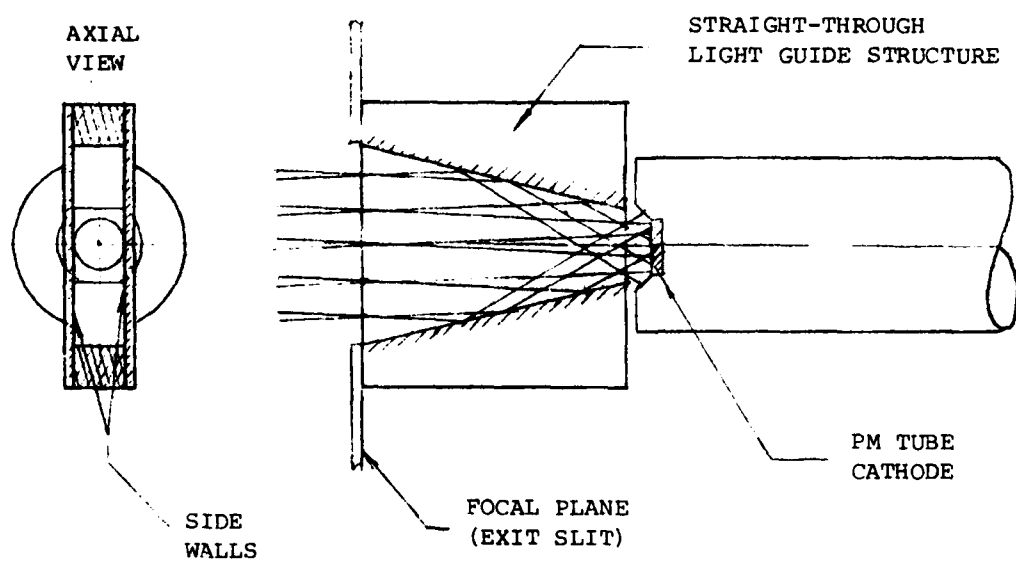STRUCTURE

SIDE WALLS

FOCAL PLANE

FIGURE 2   SCHEMATIC LAYOUT OF LIGHT GUIDE ASSEMBLIES

-4-

In the end, an all-aluminum construction was devised that circumvented all bonding problems. Special care was taken to achieve as good a polish as possible on the working optical surfaces, in recognition of the fact that overcoating of grazing-incidence surfaces was not feasible.

The end result of this effort was not as satisfactory as had been anticipated, especially with the beam-folding channels. As regards the straight-through channels, the use of light guides produced a net gain in effective area over that which would have prevailed without the use of a light guide, as will be seen in Section 3 below.

2.3 Spectroscopic Parameters of the System

2.3.1 Grating and Slits

The grating selected for this instrument was a 3600 groove/mm plane grating blazed for 2400 $\overset{o}{A}$ in the first order (blaze angle: $25^{o}36'$). The system was designed for use in the 2nd order over the spectral region of interest. This provided the double advantage of increased sensitivity, by permitting a larger entrance slit width for any given spectral passband as well as permitting the use of the 2537 $\overset{o}{A}$ Mercury line for alignment. This obviated the time consuming and excessively costly operation in a vacuum environment.

The system yielded a dispersion of 2.5 $\overset{o}{A}$/mm. Thus, by using a slit width of 4mm, a spectral bandpass of 10 $\overset{o}{A}$ (FWHM) was achieved. The slit height was 20mm, yielding an entrance aperture of 80 mm^2. To avoid optical vignetting, an aperture plate having dimensions of 35mm x 43mm was placed in front of the mirror. Thus the system solid angle field of view departed slightly from having a square shape: the horizontal f/numbers being 11.6 and 14.3, respectively.

2.3.2 Optical Aberration

The system exhibited excellent imaging qualities for all channels. The blur circle at the extremes was calculated to be less than 0.18mm diameter. This was verified by experiment.

The particular blur circle that emerged from the design effort represented a compromise with regard to the location of the grating. Ideally, minimum astigmatic blur is achieved (Ref. 1) when the grating is placed at a distance of 0.85f (where f is the mirror focal length). This would have required a much more cumbersome mounting assembly, and also would have reduced the system throughput by introducing vignetting. The distance selected for this design was 0.92f.

2.3.3 Distortion of Spectra

Because the entrance and exit slits are respectively above and below the horizontal mid-plane of symmetry, the rays incident upon and reflected from the grating are skewed with respect to the grating

normal. Under this condition the spectra are dispersed along a conic-surface with its axis about the zero order (Ref. 2). This means that the spectra lie along a hyperbola in the plane of the exit slit. A corrolary aspect of this phenomenon is that the images of the entrance slit, which lie along a separate set of orthogonal hyperbolae, are tilted with respect to their common object. The tilt angle (α) for this effect can be calculated from the following formula (Ref. 3)

$$\alpha = \tan^{-1} \left[\frac{n\lambda \tan \theta}{b \cos\beta \cos\theta} \right]$$

where
- $\lambda \equiv$ wavelength
- $n \equiv$ spectral order
- $b \equiv$ grating constant
- $\theta \equiv$ elevation angle between the ray from the central point of the entrance slit and the horizontal mid-plane (the grating normal)
- $\beta \equiv$ azimuthal angle for 1200 $\overset{o}{A}$ light measured from the grating normal

The entrance slit was located 50mm above the horizontal mid-plane; thus $\tan \theta = \frac{50}{500} = 0.1$ ($\theta = 5.71^{o}$). Inserting the remaining values into equation (1), namely:
$$n = 2$$
$$\lambda = 1200 \; \overset{o}{A} \; (= 1200 \times 10^{-7} mm)$$
$$\beta = 23.719^{o}$$
$$b = 1/3600 = 2.77 \times 10^{-4} mm,$$

one finds
$$\alpha = \tan^{-1} \left[\frac{2 \times .12 \times 10^{-3} \times 0.10}{2.778 \times 10^{-4} \times 0.9155 \times 0.995} \right]$$

$$= 5.42^{o} \; .$$

Owing to the relatively small total spread in wavelength, the hyperbolic shape of the dispersion curve was unnoticeable, so that it was not necessary to take this factor into account. By the simple expedient of tilting the entrance slit through an angle of 5.42^{o} with respect to the vertical in the opposite sense, the spectral images were returned to a vertical orientation.

2.4 Thermal Effects upon the Mirror

Because of the extensive temperature range to which the system would likely be exposed, special attention was given to the effect of differential expansion upon the mirror mounting assembly as well as the possibility of defocussing. With respect to the latter, our calculations indicated that the worst-case change in focal length would be 0.44mm from differential expansion between pyrex and aluminum. Since this would reflect itself in only a 20% increase in blur circle, no compensation measures were thought necessary.

A second area of concern was the change in radius of curvature of the pyrex mirror material itself. This was found to produce a maximum change in focal length of 0.48mm, and hence could likewise be ignored.

With regard to the mounting assembly however, the anticipated differential expansion of 0.29mm dictated that a rubber gasket be used to take up the slack.

2.5 Detector Modules

Each module contained an EMR 510G photomultiplier tube within an encapsulated parallelepiped structure as noted in the introductory section above. A high-voltage power supply, pulse amplitude discriminator, and pulse amplifier, as well as a means for varying the power supply output voltage, and a means for sending test pulses through the system via the GSE unit, was also included within the module. A plateau curve was determined to establish the most suitable operating point for each module.

These modules were also subjected to a series of vacuum tests prior to assembly within the system. A very slight sensitivity to reduced pressure was observed in one of the modules. This manifested itself as a momentary slight increase in false counting rate at a given atmospheric pressure point (few mm Hg). Since this occurred reproducibly as the device was cycled through that pressure range, the effect was judged to be inconsequential.

3.0 SYSTEM CALIBRATION

3.1 General

The system was subjected to all the requisite environmental tests without incident. In addition, a preliminary series of VUV spectral throughput tests were conducted at the AFGL VUV facility. Although this facility lacked certain features that were essential to the task of mapping the slit response and grating response of the system, it nevertheless was useful for checking that the design passband of the system ($\sim 10\text{Å}$ FWHM) was in fact achieved. Also discovered during these exercises was the excessive scattering properties of the grating discussed previously.

Upon completion of these preliminary tests, the equipment was taken to the VUV calibration facility at Johns Hopkins University, to conduct a mapping of both the slit and the grating, as well as an absolute calibration of the instrument. The facility featured a calibrated f/80 beam with exit slit dimension of 0.25mm x 2.0mm. The beam could be controlled in four degrees of freedom independently: vertical and horizontal translation and, at any point both vertical and horizontal rotation. Its passband (FWHM) was 5 $\overset{\circ}{A}$.

3.2 Scattered Light Channel

The tests performed at Johns Hopkins corroborated the earlier suspicions of excessive scattering from the grating. Thus a 1mm-thick CaF_2 filter was inserted in front of the entrance slit before the final absolute calibration. This material attenuates the 1216 $\overset{\circ}{A}$ radiation by an amount which depends upon its temperature, (e.g., at 273 $^{\circ}K$, about 0.7% of the incident light is transmitted, whereas at 195 $^{\circ}K$, about 18% is transmitted)(Ref. 4). However at 1200 $\overset{\circ}{A}$ virtually 100% of Lyman α radiation is attenuated. Thus the 1200 $\overset{\circ}{A}$ channel was sacrificed, and dedicated instead to the measurement of scattered light. This was deemed prudent by the fact that at 1304 $\overset{\circ}{A}$, (which is transmitted with little attenuation by CaF_2 relatively strong emission rates can be expected under auroral excitation conditions. Levels as high as 5 kilorayleighs have been reported (Ref. 5). This proved to be a useful measure permitting lower limit estimates of the observed emission rates to be established.

3.3 Calibration

3.3.1 Technique Adopted

An extensive series of tests was performed at the Johns Hopkins facility to achieve a reliable calibration of the instrument. The use of light guides represented a relatively new and untested approach to the problem of enhancing system sensitivity, so that this aspect was given special attention in the test plan. Of equal importance was the concern about the uniformity of the grating efficiency across its active area. The grating area was broken down into over 100 elements of area, and it was planned to collect data at each of these sites with the probe beam at the center of the entrance slit for each of the monochromator channels. In addition, a series of about 10 horizontal slit scans spanning the entire height of the slit, was planned for each of 9 different positions on the grating. These latter represented: 1) the four corners where the greatest proportion of rays passing through the light guide would impinge upon the vertical walls in grazing incidence, in addition to striking the upper or lower slanted surfaces thereof, 2) the center, and 3) the four intermediate positions, top-center, bottom-center, left-center and right-center, respectively.

This was repeated for the 1325 Å, 1356 Å and 1384 Å channels. In all instances absolute input fluxes were recorded. One of the major origins of uncertainty in absolute calibration lay in the difficulty of finding a suitable source of radiation for every channel. Ideally, one would like to find either a smooth continuum, or a single line very near the center of the system passband. However this ideal was rarely achieved. For example, in the case of the 1384 Å channel calibration, the platinum lamp that was used produced two lines: one at 1378 Å and the other at 1383 Å. Another example occurred in calibrating the 1325 Å channel, wherein the lamp again produced two lines: one at 1323 Å and a second at 1327 Å. In the case of the 1325 Å channel, this difficulty was reflected in calibration uncertainties of about ±13%. This uncertainty value was itself ascertained by a less-than-ideal method, namely: from two data sets comparing the input photon fluxes determined from the calibrated source with the observed channel counting rates on two separate occasions, all other parameters being constant. In the case of the 1384 Å channel the difficulty did not seem to manifest itself in terms of large differences in throughput, (two separate measurements yielding uncertainties of about ±5%). The 1356 Å channel on the other hand, though not exhibiting this type of difficulty, nevertheless yielded an uncertainty slightly larger than that of the 1325 Å channel. In this instance it was possible to obtain four separate readings with two different light sources: a platinum lamp and a krypton source. From these four readings an uncertainty of ±16% was ascertained.

A much greater quantity of data has been collected and recorded on tape which will eventually permit this ingredient of uncertainty to be diminished significantly. The data reported here is exclusively of a quick-look character, being limited by information recorded by hand, in real time, at the calibration site. In a similar vein, the information presented below results from hand calculations alone.

3.3.2 Calibration Results

The end-in-view of the entire calibration exercise is to produce a single number for each monochromator channel that converts the observed photon counting rate to rayleighs. From the definition of the rayleigh (10^6 photons cm^{-2}(column) sec^{-1}) it follows that a photon counting system whose field of view is filled by a uniform source of unit emission rate, i.e., one rayleigh, will experience a counting rate, C, counts per second given by:

$$C = \left(\frac{10^6}{4\pi}\right) \left(\Omega\right) \left(A'\right) \left(QT\right) \quad . \quad . \quad . \quad . \quad . \quad . \quad . \quad (2)$$

where $\Omega \equiv$ solid angle field-of-view of the system projected into object space

$A' \equiv$ the effective area of the entrance optics

$QT \equiv$ the product of quantum efficiency of the PM detector photocathode and system transmission.

The quantity, Ω, of the system is well defined, being determined by the area of the aperture plate located immediately in front of the mirror, divided by the square of the focal length of the system. The quantity A' is, under ideal conditions, given by the area of the entrance slit. However, this ideal situation presumes that the system transmission loss is uniform for all points in the slit and all points of the grating. Since this ideal is far from realized, and because the slit factors and grating factors are intertwined with one another, it was found convenient to lump this mix of loss factors into two separate and readily identifiable factors namely: 1) the effective slit area, and 2) the QT factor for the center of the grating and the center of the slit, as follows.

As noted previously, a series of measurements was conducted in which the entrance slit was scanned at about 10 different levels for each of nine different positions of the grating, while ensuring that the light source remained constant within acceptable limits of a few percent. A complete reduction of all these data would involve an effort that is clearly well beyond the scope of this contractual obligation.

Instead an alternate simplified approach was adopted that was more amenable to hand reduction. It was noticed that in all cases the light guide acted as though there were in existence an upper and lower mirror which effectively tripled the actual area of the detector. This tripling effect was in fact almost fully realized for only a few of the orientations, namely those where the input light beam impinged at the center of the grating. In all other cases the upper and lower images were rather heavily attenuated due to reflection losses in the light guide mirror surfaces. Nevertheless, an inspection of the analogue strip chart recording permitted a reasonably accurate assessment of this effect. Thus it was possible to assign a single attenuation factor to both the upper and the lower images for the various input directions. These data were expressed as a multiplying ratio

$$M' = \frac{\sum_{i=1}^{3} S_i}{S_2} \qquad \ldots \ldots \ldots (3),$$

where S_1 $\equiv$ the observed average signal
level for the lower image

S_2 $\equiv$ the signal level for the
central image

S_3 $\equiv$ the signal level for the
upper image

for each orientation. An average of the several M'-values was then
taken to derive a composite M-value for each wavelength channel.
The effective area was then calculated by taking the product of M
and the area of the photocathode unobstructed by the light guide.
(The actual area of the cathode is $32.12mm^2$, whereas the unobstructed
area is $28.3mm^2$).

Table I lists the values obtained by following the above
procedure.

TABLE I

Effective area ratios derived
from the analogue chart
slit function calibration data

λ	M	A'
1325 $\overset{o}{A}$	1.75 ±0.18	0.49 cm^2 ±0.051
1356 $\overset{o}{A}$	1.60 ±0.13	0.453 cm^2 ±0.037
1384 $\overset{o}{A}$	1.61 ±0.22	0.455 cm^2 ±0.062

The uncertainties listed in Table I were obtained by simply
computing the RMS value of the several data points from which each
listed average value was comprised.

The QT-values obtained with the f/80 beam passing through the
center of the slit and oriented so as to fall on the center of the
grating are listed in Table II together with the C-values calculated
from Equation (2). These values were obtained by simply taking the
appropriate counting rate reading, and dividing by the calibrated
photon flux entering the system, expressed in counts/photon. The
value of Ω is simply $(35mm \times 45mm)/(500mm)^2 = 6.02 \times 10^{-3}$ steradian.

TABLE II

CALCULATED CALIBRATION FACTORS

λ	A'	QT	C (counts/sec Rayleigh)	Rayleighs counts/sec
1325 Å	0.49	$(6.91 \pm 0.89) \times 10^{-3}$	1.62 ±0.27	0.62 ±0.11
1356 Å	0.453	$(1.21 \pm 0.19) \times 10^{-3}$	0.260 ±0.046	3.85 ±0.70
1384 Å	0.455	$(4.40 \pm 0.20) \times 10^{-3}$	0.951 ±0.136	1.05 ±0.307

The last column on the right of Table II represents the desired end result of the calibration exercise. The uncertainties listed were calculated on the assumption of stochastic independence of the contributory factors. This is thought to be a reasonable basis for calculation for the following reasons: the A'-values were obtained over a relatively short period of time during which the calibrated input source did not exhibit any appreciable variation. Hence the listed uncertainties in A'-values reflected point-to-point variations in the monochromator proper. The total counts in all cases was large enough so as to render counting statistics fluctuations inconsequential. The listed QT-value uncertainties, however, were based upon two or more measurements using different lamp sources under less than ideal conditions but with all monochromator probe parameters held constant and are therefore not believed to be related to the monochromator proper.

It is perhaps instructive to examine the relative contributions to the overall uncertainties. These are shown in Table III below; the last column on the right is the square root of the sum of the squares of the previous two columns.

TABLE III

RELATIVE CONTRIBUTION TO CALIBRATION UNCERTAINTY

λ	$\dfrac{\delta A'}{A'}$	$\dfrac{\delta(QT)}{QT}$	$\dfrac{\delta C}{C}$
1325	0.104	0.129	0.165
1356	0.082	0.157	0.177
1384	0.136	0.045	0.143

From a brief perusal of the data in Table III, it can be concluded that any efforts to improve the absolute uncertainties inherent in the monochromator would quickly arrive at the point of diminishing returns (except for the 1384 Å channel) unless a concomitant effort were mounted to reduce the uncertainties in the input photon fluxes.

4.0 DISCUSSION

The instrument collected auroral emission data on the rocket flight
flown in early March of 1981 attaining an apogee of 158 km. Although the
data have not as yet been reduced and analyzed in detail, we have been able
to examine the quick-look results in a perfunctory fashion and to draw some
preliminary conclusions. Our examination was conducted within the context
of assessing whether useful information could be derived in the presence of
excessive scattered radiation from known line radiation. Needless to say,
although this is answered in the affirmative, the results would have been
much less speculative had scattering been avoided. In this connection we
feel also obliged to assert that this can be corrected in any future endeavor
of this kind.

As explained previously, the 1200 $\overset{\circ}{A}$ channel was dedicated to observing
the magnitude of this effect. A plot of the output of this channel is shown
in Figure 3. The abscissa is in units of seconds, while the ordinate is in
units of counts per 100 milliseconds. Each point in the plot represents a
best fit to a cubic over an interval of ±5 seconds about the point. The
vertical lines are marked with the designated rocket altitude in km.

The first, low-level non-zero counting rate peak extending from a few
seconds to about 65 seconds is spurious, associated with rocket engine and
dynamic pressure effects. The nose cone was ejected at 82 seconds. The
initial rise and inflection point occurring at about 90 seconds is most
likely due to Lyman-α radiation, which can penetrate to the altitude levels
attained up to this time, (e^{-1}-value occurring at about 75 km). Beyond this
time this radiation is not expected to increase appreciably because of the
relatively large atomic hydrogen scale height that prevails above 100 km.
Beyond this altitude the signal level rises much more precipitously, and
after experiencing a brief peak value of about 35 counts per second at about
110 second (which is believed to evidence spatial variations along the path
of the payload), the signal levels off to a reasonably constant value
throughout the remainder of the flight. The precipitous rise commencing
at about 100 km, close to the e^{-1}-penetration level for 1304 $\overset{\circ}{A}$ radiation, is
believed to be due to this component.

From perfunctory tests performed at the Johns Hopkins facility to assess
the relative response of the various channels to scattered radiation lying
outside their respective passbands, we have good reason to believe that the
contribution of scattered light to the other channels would be roughly com-
parable to the value observed in this channel. Pursuing this reasoning, it
is possible to place upper and lower bounds upon the derived difference
signal levels in the remaining channels.

The differencing procedure followed in our analysis is exemplified by
the plots shown in Figure 4. The upper curve is a direct plot of the 1325 $\overset{\circ}{A}$
channel signal. The lower, dashed curve is a replica of the 1200 $\overset{\circ}{A}$ scat-
tering channel, normalized to the lowest excursion of the upper curve. The
logic underlying this procedure proceeds from the presumption that 1) the
scattered light level cannot be less than the lowest excursion, and that 2)
the temporal variations of the scattered light component will be the same
in all channels. Pursuing this line of reasoning, the difference signal
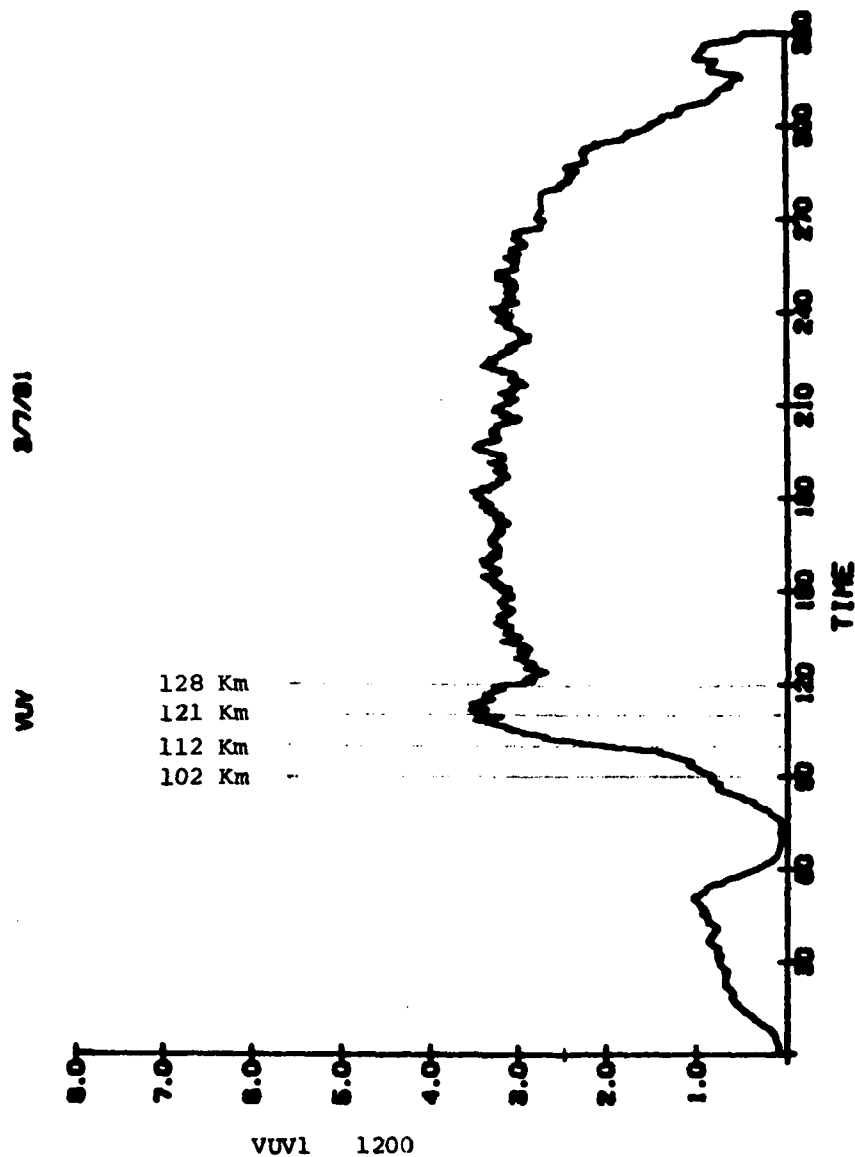
FIGURE 3: Scattering channel output as a function of time.
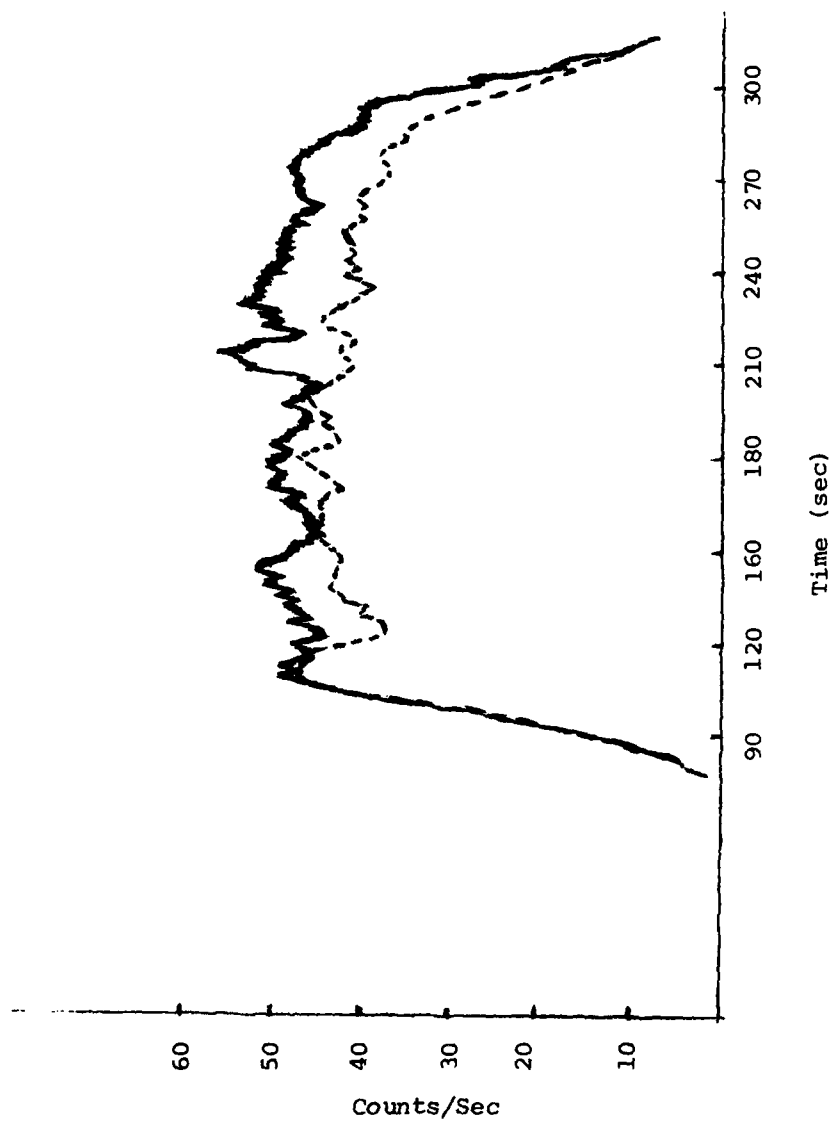
Figure 4:   Illustration showing the derivation
            of the difference signal for each channel.

lying between the two curves represents the lower limit of emission rate pertaining to this channel. The upper limit is of course the value obtained on the presumption of zero scattering. However it is believed that the actual signal levels are much closer to the lower limit values, based upon the scattering tests at Johns Hopkins.

The minimum values for the 1325 Å, 1356 Å, and 1384 Å channels, respectively were determined in the same manner, and are depicted in Figure 5. The vertical grid lines are designated and marked with the appropriate altitudes. The left-hand scale is in units of counts per sec, whereas the right-hand scale is in units of rayleighs taken from the calibration data for each channel. The jaggedness of the curves is not intended to depict the actual noise, but merely reflects an attempt at a visual representation simulating the noisiness of the signal.

In this latter connection it should be pointed out that the zero value shown in the 1384 Å channel during the 28-second period between 171 seconds and 199 seconds, is a continuous sequence of data points where the normalized scattering signal was found to be equal to the 1384 Å signal level over this entire time span. This particular finding lends added credence to the suggestion that the longer-period jagged structure, of period greater than 5-10 seconds, represents valid data, and that the higher frequency noise component is perhaps not much larger than the simulated amplitudes depicted in these figures.

Two features stand out clearly in the figure: 1) the tendency for exhibiting a trough toward the middle which seems to be more pronounced in these difference signals than in the scattering channel, and 2) the generally higher emission rates for the 1356 Å channel.

With regard to the latter item, it is noted that this channel includes light originating from the LBH (3,0) transition of the nitrogen molecule, while the 1325 Å and 1384 Å channels are derived from the (4,0) and (2,0) transitions, respectively (Ref. 6), which bracket the other. Thus it should be possible to arrive at a meaningful estimate of the N_2 contribution to the 1356 channel.

The suggestion of a somewhat deeper trough in the 1356 channel is a bit puzzling, in that one might have anticipated a lesser trough owing to the fact that the atomic oxygen density scale height between 120 and 160 km is almost twice that of N_2. Also, the scattering channel, which for reasons already cited appears to be comprised mainly of atomic oxygen signal from 1304 Å, corroborates this hypothesis by not evidencing a trough.

On the basis of these differences, it is interesting to speculate on the possibility that the 1304 Å radiation originates from oxygen atoms that are excited at altitudes above apogee (∿160 km), whereas the 1356 Å radiation might originate from excitation of oxygen atoms at lower altitudes. Perhaps the electron spectra may shed further light on this speculation. Should this turn out to be substantiated, it might prove worthwhile to explore this question in some greater depth in a future experiment.
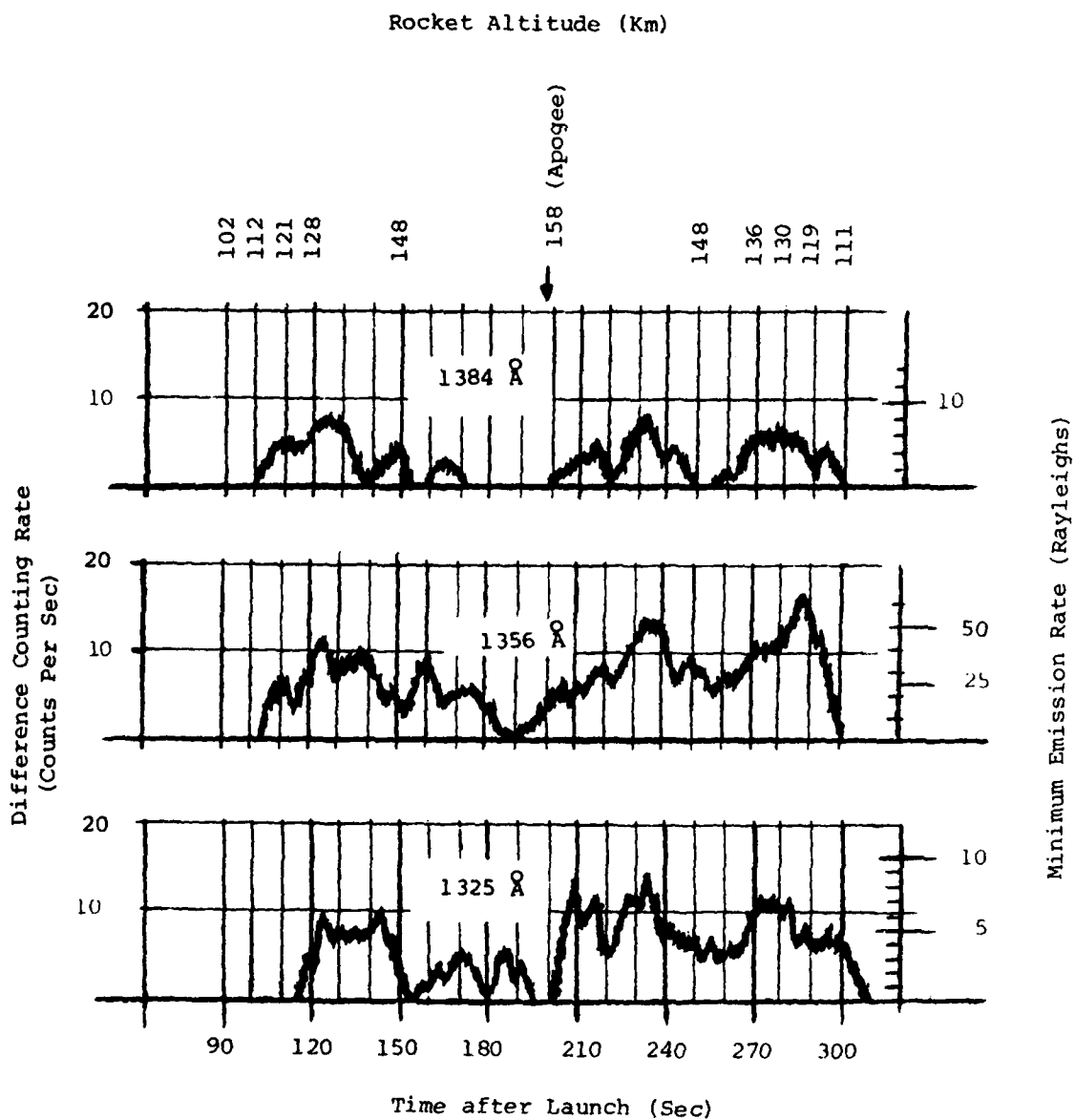
FIGURE 5: Observed lower limit
auroral emission rates.

REFERENCES

1. Mielenz, K. D., J. Res., Nat'l Bur. Stand., C. Eng. & Instr., 68C, No. 4, 205, (1964).

2. Miranda, H. A., Jr., Applied Optics, 4, 809, (1965).

3. Tarasov, K. I., "Spectralnyi Pribori", (Mashinostroenie, Leningrad, 1977), pp 69-71.

4. Handbook of Optics, W. G. Driscoll, ed., McGraw-Hill, 1978, pp 7-16.

5. Sharp, W. E., and Rees, M. H., J. Geophys. Res., 77, 1810 (1972).

6. R. E. Huffman, F. J. LeBlanc, J. C. Larrabee, and D. E. Paulsen, J. Geophys. Res., 85, 2201 (1980).

7-8